Empirical Model for the Description of Weld Seam Geometry in Coaxial Laser Hot-Wire Deposition Welding Processes with Different Steel Wires

Laura Budde[1] · **Kai Biester[1]** · **Michael Huse[1]** · **Marius Lammers[1]** ·
Jörg Hermsdorf[1] · **Ludger Overmeyer[1]**

Abstract

Claddings are used to protect areas of components that are exposed to particular chemical, physical or tribological stresses. The aim when developing a cladding process is to achieve a cladding with low waviness in order to reduce the amount of machining required. Computational models and FEA simulations can be used to determine process parameters for claddings with low rework including a prediction of the height and width of a single weld seam aswell as the development of welding strategies. In this paper empirical models describing the geometry of single weld seams on a substrate manufactured with a coaxial laser hot-wire cladding process are investigated for three steel wire materials and different welding parameters. The coordinates of surface points of the weld seams were detected using a laser scanning microscope and post-processed by a self-created script. In order to describe the cross sectional shape of the weld seams, the parameters of parabolic, cosinusiodal or circular arc model functions are derived from the surface data using a fitting algorithm. For the tested wire materials, an effect of the wire material on the shape of the weld seam was not observed. The investigations also show that regardless of the varied welding parameter set or wire material, a circular model function appears to be the most suitable model shape for describing the cross sectional weld seam geometry in coaxial laser metal deposition with hot-wire. The regression residua using a circular arc model function ranged from 18.9 µm to 34.6 µm, which indicates a good approximation.

Keywords Laser metal deposition with hot-wire · LMD-W · Cladding · Weld seam geometry · Empirical model

✉ Laura Budde
l.budde@lzh.de

1 Laser Zentrum Hannover e.V, Hollerithallee 8, Hannover 30419, Germany

Introduction

Cladding processes are used in various applications to improve the mechanical and chemical properties of the surface of a stressed component as well as to repair worn or damaged components. For the production of protective claddings with a thickness of about 1 mm, different processes are known like laser metal deposition with powder (LMD-P), laser metal deposition with wire (LMD-W), plasma transferred arc welding (PTA), wire and arc additive manufacturing (WAAM) and electron beam melting (EBM) [1–3]. These processes are characterized by adding layers of overlapping weld seams to the base material. In order to obtain high-quality protective layers with low substractive post-processing efforts, the position of the weld seams has be chosen carefully, in a way that a constant layer thickness and a stable welding process is achieved. At the same time the waviness of the cladding surface has to be kept low in order to avoid high reworking costs. When designing such processes the precise knowledge of the shape of a single weld seam and the overlapping of weld seams is mandatory for finding an optimal set of cladding parameters.

Models of the weld seam geometry have already been studied before for various deposition welding processes. Ocelík et al. investigated weld seams created by LMD-P with coaxial and lateral powder feeding nozzles and compared the single-track geometry to parabolic, sinusoidal, circular arc and ellipsoidal model functions. Stainless steel was used for both the substrate and the cladding material. The laser source was a continuous wave fiber laser. As a criterion for the suitability of the model functions for describing the weld seam surface the sum of the squared residuals was evaluated. The authors found the parabolic shape to be most suitable for describing the weld seams shape when laterally feeding the powder. In case the powder was coaxial feed the weld seams were best described by the parabolic function while the sinusoidal function was second best. The elliptical function was in all cases most inaccurate. A geometrical model for weld seam overlap was introduced to calculate the shape of two neighbour weld seams based on the shape of the first weld seam and an overlap ratio. The model shows good agreement with experimental results [4]. Nenadl et al. investigated the accuracy of predictions of a geometrical model of single layer claddings manufactured with a LMD-P process. They found a parabolic function suitable for prediction of the overall shape. Geometry parameters of a single layer cladding surface correlated with process parameters allowing for a prediction of overlapping weld seams using the geometrical model found by Ocelik et al. The process parameters welding speed, laser power, powder feed rate and weld seam displacement as well as some experimental system design constants are input parameters of the geometry prediction [5]. Later Nenadl et al. extended the model to multi-layer claddings. Experimental results showed that the first layer behaves different than all subsequent layers. Therefore a correction of 15 % for single track height for following layers was implemented to provide accurate predictions [6]. Gonçalves et al. developed neural networks for LMD-P to compute the height and the width of the weld seam. The networks use a melt pool image and the process parameters as input parameters.

Six different neural network multi-layer designs were tested. The predictions of the networks reach coefficients of determination of 0.98 [7]. El Cheikh et al. used a multiple regression analysis method to describe the relationship between the LMD-P process parameters and the weld seam geometry parameters height, width and cross sectional area. The authors assumed surface tension to be the dominant factor in the formation of the melt pool geometry, so they only used a circular arc as a model function of the weld seam cross-section. As a result, the geometry of the weld seam surface was predicted with good accuracy [8].

Shi et al. described the relationship between the parameters of the LMD-W process and the weld seam geometry by a mathematical model. A coaxial CO_2 laser welding head was used for the generation of welding samples. The geometry of the weld seam was assumed to be circular arc shaped. A comparison between predicted cladding height, width and cross section of the mathematical model and the experimental results for different parameter sets showed the same trend, but deviations of more than 10 % were found with some parameter sets [9].

Ding et al. investigated weld seams manufactured by WAAM. Mathematical model functions were compared to experimental data derived from high resolution measurements with a 3D laser scanning system. The best fit was found for both the parabolic and the cosinusiodal model [10]. Xiong et al. showed that for WAAM processes the shape of the weld seam is influenced by the ratio of wire feed rate and welding speed. At high feed rate ratio the weld seam tends to have a circular arc shape while at low ratio the weld seam has a parabolic shape [11]. Cao et al. compared the weld seam geometry to gaussian, logistic, parabolic and sinusoidal model functions, finding the best fit for sinusoidal functions [12]. Deng et al. used machine learning to predict weld seam geometry based on process parameters. A maximum relative error of 4.29 % for weld seam width and 2.78 % for weld seam height was reported [13]. Karmuhilan et al. also investigated the weld seam geometry using an artificial neural network. Feed forward backprop neural networks were used for the prediction of weld seam geometry based on process parameters and for the prediction of process parameters for a specific weld seam. They calculated a coefficient of determination of 99.73 % for height and 99.53 % for width [14]. Xue et al. investigated the prediction of the weld seam height and width of a WAAM process based on two different neural networks. A feed forward backprop neural network was compared to a feed forward backprop neural network with a multi-population genetic algorithm for weight optimization. The prediction accuracy of the neural network with multi-population genetic algorithm was higher with a prediction error of 5.5 % [15].

In addition to empirical models describing the geometry of a weld seam, computational simulative studies are also carried out in this field of research. Wei et al. developed a computational model for the laser hot-wire cladding process. The model combines a multi-phase model for laser melting with a multi-phase model for laser hot-wire deposition. In this way, the material feed and heating by the hot-wire process and the resulting melt pool properties are combined in one model. Due to the complex gas-liquid-solid multi-phase flows in this process factors like free surface tracking, gas-liquid-solid continuum, mass addition of wire, the two external heat sources laser beam and wire preheating, melting/solidification, convective driving forces like surface tension and density gradients and

temperature dependent properties of the materials are considered in this model. Simplifications are adopted in some places. For example, the influence of the inert gas on the surface of the melt pool and on the flows in the melt pool is neglected. The influence of wire movement on the melt pool is also neglected. The model can be used to predict weld seam geometry, melt pool geometry, temperature distribution and microstructure. To validate the model, the simulation results were compared with laser hot-wire cladding tests and heat conduction welding tests. A good agreement between experimental results and simulated results was observed. A Marangoni outward flow pattern was observed for negative temperature coefficients of surface tension, which led to a uniform temperature distribution in the melt pool and a wider cladding formation [16]. Pinkerton and Li modeled the geometry of the melt pool and weld seam of a LMD-P process using energy and mass balances. The weld seam surface was considered to be a circular arc instead of an ellipse to reflect that the surface tension forces are a dominant factor in the melt pool [17]. Rios et al. investigated a WAAM process with Ti-6Al-4V as wire material. An analytical heat flow model and capillarity theory were used to establish a model for the description of the deposited geometry based on the process parameters. The model was validated through experiments. According to capillarity theory depositions with a radius of 6 mm or less can be described by a circular arc due to the fact that the surface tension forces are more dominant than the hydrostatic pressure. This was confirmed experimentally [18].

The findings so far show that the function describing the weld seam geometry depends strongly on the process, the arrangement of the system technology (coaxial and lateral feeding) and in some cases also on the process parameters. Model functions best suited to describe weld seam geometry according to previous research include the parabolic function (see [4, 5, 10, 11]), the circular arc function (see [11, 18]), and the cosinusiodal/sinusoidal function (see [10, 12]). Since the surface tension forces have a significant influence on the melt pool geometry and thus on the subsequent weld seam shape, a circular arc shape is assumed in some cases to describe the weld seam cross-section (see [8, 9, 17]). Findings on the transferability of the results to other materials besides those used are not available. A simulation model for the laser hot-wire deposition welding process was developed by Wei et al. (see [16]), but the process had a lateral wire feed and the influence of wire movement and shielding gas flow on the melt pool geometry was neglected. In the investigation of a LMD-W process Shi et al. assumed an arc shape weld seam surface, but did not verify this by comparison with other functions [9]. For this reason, this paper examines a selection of model functions having a good agreement with experimental results mentioned before in order to describe the weld seam geometry in coaxial laser metal deposition with hot-wire. The following functions are used:

Parabolic function:

$$f_{\mathrm{p}}(x) = a \cdot x^2 + b \cdot x + c \tag{1}$$

Cosinusiodal function:

$$f_c(x) = a \cdot cos(b \cdot x + c) \tag{2}$$

Circular arc function:

$$f_a(x) = \sqrt{r^2 - (x-a)^2} - b \tag{3}$$

In order to obtain a prediction on the transferability of the results to other steel materials, three different wire materials were investigated. Possible dependencies of the weld seam geometry on the wire materials can be determined in this way. The knowledge of the weld seam geometry is a prerequisite for the development of a mathematical model to predict the geometry of overlapping weld seams, which in turn can be used to predict layer thicknesses and waviness, and thus reducing the amount of experimentation required to determine appropriate parameters.

For the present study, the previously mentioned requirements are taken into account. Research questions that are addressed in this paper are as follows:

- Which of the model functions f_p, f_c or f_a describes best the cross section of a single weld seam in coaxial laser metal deposition with hot-wire?
- Does the model function type depend on the process parameters?
- Does the wire material have an influence on the weld seam geometry?

Materials and Methods

Materials

Three different cladding materials were investigated: the unalloyed steel G3Si1, the austenitic stainless steel X2CrNiMo19-12 and the martensitic valve steel X45CrSi9-3. The mild steel S235JR was used as the substrate. The alloy compositions of all materials used are shown in Table 1 and the electrical resistances in Table 2. For the austenitic stainless steel X2CrNiMo19-12 no data on electrical resistivity was available. Instead the data of the austenitic stainless steel X2CrNiMo18143, which has a very similar chemical composition, is used. Due to their similar chemical composition both stainless steels are grouped in 316L by the american standard.

Experimental Investigations

The weld seams were prepared using a coaxial laser hot-wire deposition welding head MK-II of the Laser Zentrum Hannover e.V. The laser beam source was a LDM 3000-40 continuous wave diode laser of the Laserline GmbH. The laser beam wavelength was in the range between 1020 nm and 1060 nm with a tolerance of ±15 nm and a maximum laser power of 3.0 kW. The fiber core had a

Table 1 Chemical composition in wt.% of S235JR [19], G3Si1 [20], X45CrSi9-3 [21] and X2CrNiMo1912 [22]

	C	Si	Mn	Cr	Ni	Mo	Cu
S235JR	0.05-0.14	≤0.1	0.2-0.8				≤0.2
G3Si1	0.06-0.15	0.8-1.15	1.4-1.85				≤0.5
X45CrSi9-3	0.4-0.5	2.7-3.3	≤0.6	8.0-10.0	≤0.5		
X2CrNiMo19-12	0.013	0.873	1.709	18.3	12.22	2.641	

Table 2 Specific Electrical resistance of G3Si1 [23], X45CrSi9-3 [21] and X2CrNiMo18-14-3 [24]

Material	Specific electrical resistance	Reference temperature
	$\rho_{el} / (\Omega\cdot mm^2/m)$	$T_{ref}/°C$
G3Si1	0.34	44
X45CrSi9-3	0.90	20
X2CrNiMo18-14-3	0.75	20

diameter of 400 µm. The collimator had a focal length of 100 mm and the focusing lens a focal length of 300 mm. Within the processing head, a lens guides the laser beam onto a regular square pyramid. The reflectively coated pyramid faces split the laser beam into four partial beams and deflects them to the outside. The partial beams are reflected by deflecting mirrors and guided to a common focal point at the tip of the wire. By splitting the laser beam into the partial beams, the wire and the media hoses can be supplied into the processing head to the welding nozzle and an arrangement where the welding wire can be fed coaxial into the processing zone with the four partial beams combined in one focal area can be used [25]. Figure 1 shows the principle of the laser beam path. In contrast to a lateral arrangement of the welding wire, this offers the advantage of an at least approximate directional independence during welding. The experimental setup is shown in Fig. 2.

Substrates

Flat steels with thicknesses of 10 mm and 10.3 mm, a width of 40 mm and a length of 160 mm were used as substrate for the experiments. For the welding experiments with a X2CrNiMo19-12 or a G3Si1 wires the thicknesses of the flat steel substrates were 10.0 mm and 10.3 mm for X45CrSi9-3 wires. The difference in thicknesses were due to a different substrate material batch and caused a variation of the stickout length. The latter is defined as the distance between the welding nozzle and the workpiece surface. A variation of the stickout length influences the preheating of the
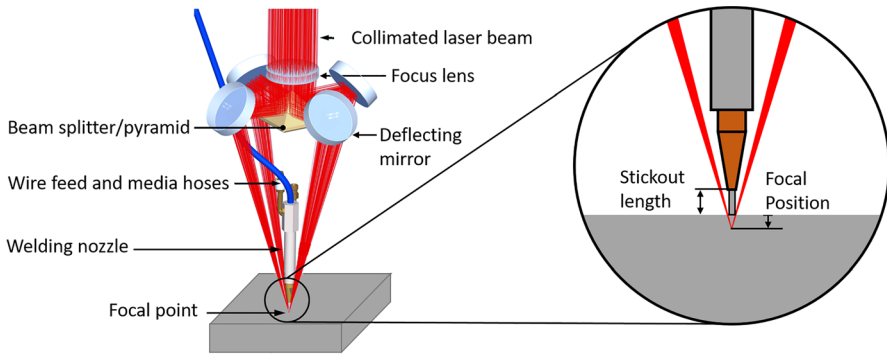
Fig. 1 Beam path in the welding head MK-II and detailed view with process parameter definition

wire as well as the laser spot diameter. The thickness variations were detected after the preparation of the specimen and were thus considered in the evaluation. Before welding the substrates were sandblasted and cleaned with ethanol but not preheated.

Preheating of the Wire

The current intensity for an electrical preheating of the wire was adjusted to the planned stickout and to the material of the wire. A relationship between electrical heating power P_{el}, voltage U, electrical resistance R, stickout l_W, specific electrical resistance of the material ρ_{el}, wire diameter d_W and electrical current I is given by
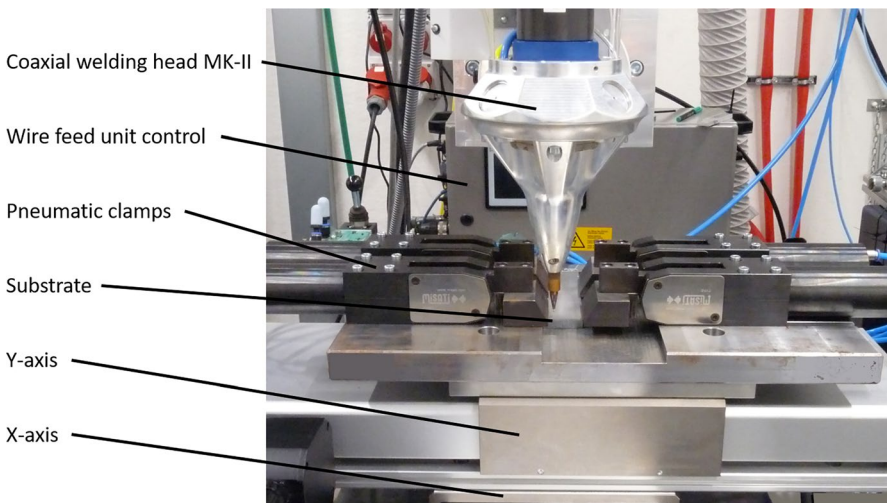
Fig. 2 Experimental setup for coaxial laser hot-wire deposition welding

Joule's law below. It was used by Pajukoski et al. to compute the preheating of the wire material [26]:

$$P_{el} = U \cdot I = I^2 \cdot R = \frac{4 \cdot I^2 \cdot \rho_{el} \cdot l_W}{d_W^2 \cdot \pi} \qquad (4)$$

Experimental Design

Beside the wire materials and the stickout length l_W also the welding speed v_S and the preheating current of the wire I were varied in this investigation, while the wire feed speed v_W, the shielding gas flow rate $\dot{V}$ and laser power P_L were kept constant. The welded seams had a length of 60 mm.

According to Eq. 4 the term $I^2 \cdot \rho_{el} \cdot l_W$ has to be constant in order to keep the preheating power and thus the temperature of the wire constant for a given wire material combination. Due to the lower electrical resistance of G3Si1, a higher current was required for the corresponding welding experiments. The current for the welding tests with larger stickout are calculated based on Eq 4:

$$I_2 = I_1 \cdot \sqrt{\frac{l_{W,1}}{l_{W,2}}} \qquad (5)$$

Table 3 Overview of the process parameters

Process parameter	Value
Wire feed speed v_W	2.0 m/min
Laser power P_L	2.1 kW
Shielding gas	Argon
Shielding gas flow rate $\dot{V}$	8.0 l/min
Wire diameter d_W	1.0 mm
Stickout length l_W	6.5 mm; 7.0 mm (X2CrNiMo19-12)
	6.8 mm; 7.3 mm (G3Si1 & X45CrSi9-3)
Focal position z_L	2.25 mm; 2.75 mm (X2CrNiMo19-12)
	2.45 mm; 1.95 mm (G3Si1 & X45CrSi9-3)
Spot diameter on substrate w_L	3.0 mm / 2.3 mm (X2CrNiMo19-12)
	2.66 mm; 2.15 mm (G3Si1 & X45CrSi9-3)
Current I	
G3Si1	110 A; 106 A
X45CrSi9-3	80 A; 77 A
X2CrNiMo19-12	80 A; 77 A
Welding speed v_S	1200 m/min
	950 m/min
	700 m/min

The other welding parameters were determined on the basis of findings in previous investigations. For each parameter combination a stable process was observed. An overview of the parameters is shown in Table 3.

A full factorial design with three repetitions per parameter set was chosen as experimental design. It allows the determination of all interactions and a good statistical validation of the results. The experiments are performed in a partially randomized manner. Due to the increased effort involved in changing the wire, the wire material is used as a block factor for generation of the experimental design.

Recording of the Actual Wire Feed Speed

During welding the actual wire feed speed $v_{W,act}$ is recorded by the Dinse wire feed unit. This is subsequently compared with the set wire feed speed. The data is used to calculate the cross section A_{100} of the weld seam, which assumes a 100 % utilization of the welding wire and thus assumes no effects like alloy burn-off and deviations from the planned wire diameter. It is calculated based on wire feed speed and welding speed v_S according to the following equation [9]:

$$A_{100} = \frac{v_{W,act} \cdot d_W^2 \cdot \pi}{4 \cdot v_S}$$

(6)

3D-scan with Laser Scanning Microscope

In order to evaluate the welded seams for the most appropriate model function f_p, f_c or f_a, the geometry of the weld seams was measured using a Keyence VK-X 1100 laser scanning microscope. The surface was scanned in the focus variation mode, which has a height dependent vertical accuracy of $\delta z = \pm(1.0 + \text{measured height}/100\,\mu m)\,\mu m$ and a resolution of 0.5 nm for height measurements. The measured data of the weld seam surface was exported in STL-files for post-processing
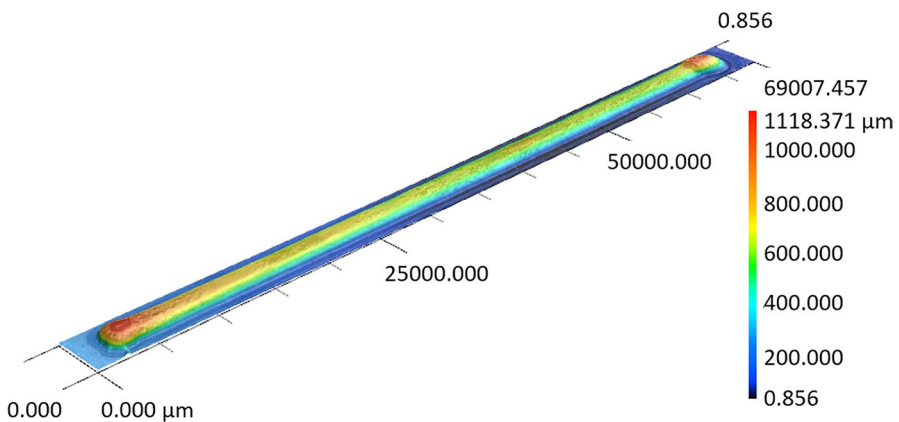

Fig. 3 Weld seam surface measured with the laser scanning microscope
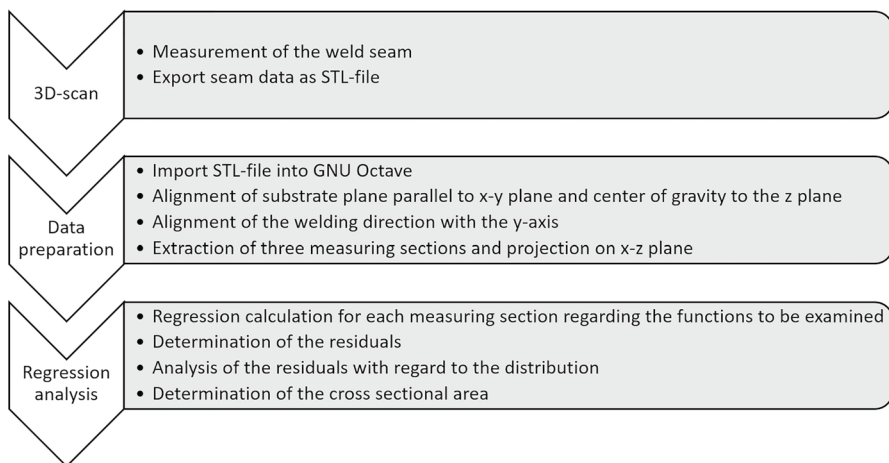
in further programs. The recorded files of the weld seam contain approximately 10 million data points, which were reduced and divided in following processing steps. An example of a surface scan of a weld seam is shown in Fig. 3.

Data Analysis and Regression

Before evaluating the surface data for most suitable model function based on a regression analysis the data was prepared and evaluated according to the workflow shown in Fig. 4. Each processing step of the data described in the following text was done using scripts in the GNU Octave software.

Data Preparation

The first preparation step was to align the substrate surface parallel to the x-y plane. In order to calculate the alignment transformation, the set of points read from a STL file is divided into two subsets, the substrate points and the the deposited material points. As a separation criterion the z component of each point was used. All data points with z components within a tolerance band of size Δ above the overall minimum z of all points were assigned to the substrate point subset while all remaining points were categorized as deposited material points, the weld seam points. The value of Δ was chosen using visualizations of the point subsets, trying to cover all substrate points using a high Δ value and at the same time, keeping Δ as low as possible in order to exclude weld seam points. This method was neccessary due to the slight inclination of the data with respect to the xy-plane, which resulted from welding distortion. The inclination caused an overlap of the heights of some positions on the weld seam edge with the heights of the substrate material. As a result a tolerance of $\Delta = 0.17$ mm was found and applied throughout this investigation. Based on the

3D-scan
- Measurement of the weld seam
- Export seam data as STL-file

Data preparation
- Import STL-file into GNU Octave
- Alignment of substrate plane parallel to x-y plane and center of gravity to the z plane
- Alignment of the welding direction with the y-axis
- Extraction of three measuring sections and projection on x-z plane

Regression analysis
- Regression calculation for each measuring section regarding the functions to be examined
- Determination of the residuals
- Analysis of the residuals with regard to the distribution
- Determination of the cross sectional area

Fig. 4 Workflow of data acquisition, preparation and evaluation

points of the substrate subset the determination of a subset plane was performed by minimizing the square of the normal distance of the substrate points from the plane. The angle between the normal vector of the subset plane and the z-axis was used in a rotation matrix to adjust all data points parallel to the xy-plane, after shifting the center of gravity of all data points to the origin of the coordinate system.

After the alignment with respect to the xy-plane, the weld seam points were aligned in the direction of the y-axis, which is in accordance with the welding direction. The algorithm used divides the weld seam points into an initial section, a middle and an end section according to their y-coordinate. In order to prevent effects at the start and at the end of the weld seam only points from the middle sections were used to find an appropriately aligning transformation. Of all the points of the middle section only weld seam points were used, whose z-coordinate was larger than the above tolerance Δ over the middle sections overall minimum z. In the next step, the middle section is divided in intervals of 0.2 mm length along the y-axis. In every interval the average of the x-components of the intervals crest points were computed, whose z-component was larger than the overall maximum z minus 0.1 mm. The average x and the middle y-coordinate of every interval were then used to determine the crest line in a regression. An example of the resulting points and the crest line is shown in Fig. 5.

From the angle between the crest line and the y-axis a rotation matrix was calculated which aligns the data points parallel to the y-axis. This matrix was applied to all data points. Additionally, the data points were translated so that the crest line has an x-axis intersection at 0 and the highest point of the weld seam is approximately the intersection of the model function with the z-axis. The data points shift makes the graphical representation of the data always appear at the same position in the coordinate system. A further shift is not necessary for fitting the model functions.

After the data points of the weld seam have been arranged appropriately in space for further analysis steps, the next step was to divide the middle section into three
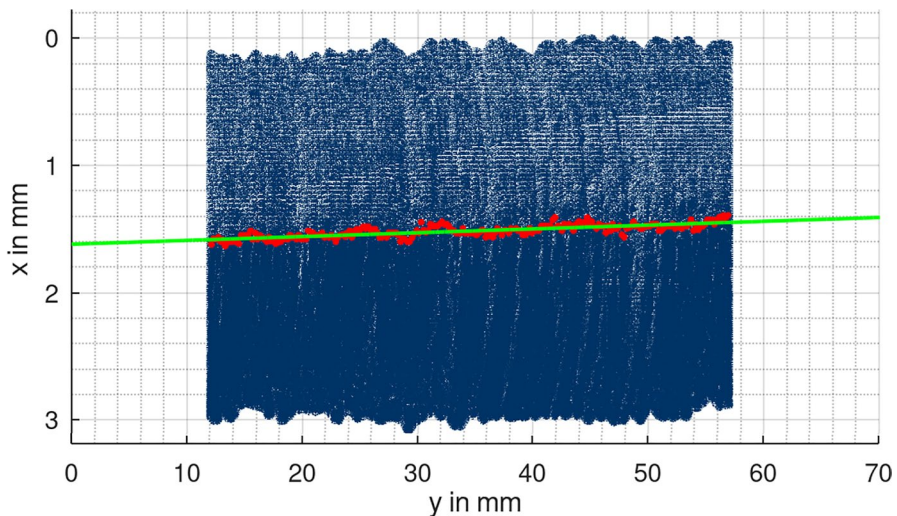

Fig. 5 Regression line (green) with the points of the means (red) in measurement data (blue)

subsections, each with a length of 15 mm. By dividing the weld seam into several subsections, the influence of distortion in the longitudinal direction of the weld seam can be minimized. The last step of the data preparation was the projection of the data points of each subsection onto the xz-plane. Every subsection contains approximately 1.5 million data points which form a sufficient base for fitting the model functions to the data points and thus determining the model functions parameters. An example for an aligned and divided weld seam is shown in Fig. 6.

Regression Analysis

For each of the projected subsection points the fitting of the model functions was carried out using the Levenberg-Marquardt algorithm. This algorithm is widely used to solve nonlinear least squares problems and combines the Gauss-Newton method and the gradient descent method. The gradient-descent method is dominant for parameters far from the optimal value while the Gauss Newton method is dominant for parameters close to the optimum [27]. The Levenberg-Marquardt algorithm is very robust and converges with high probability even under poor initial conditions. As a measure of the quality of the regression the standard error of regression (SER) was determined depending on material, welding speed and stickout length. In this way, a function can be determined which is best suited to describe the weld seam surface. The coefficient of determination R^2 was not calculated, since it has limited significance for nonlinear regression functions.

The two zeros x_{01} and x_{02} as well as the cross sectional area A_M were calculated for the model functions (Eqs. 1, 2, 3) of each subsection. The cross section A_{100} for each weld seam is also determined using the actual wire feed speed $v_{W,act}$ and Eq. 6 and compared to A_M of the model function, to verify whether the assumption of 100 % utilization of the wire material can be confirmed.
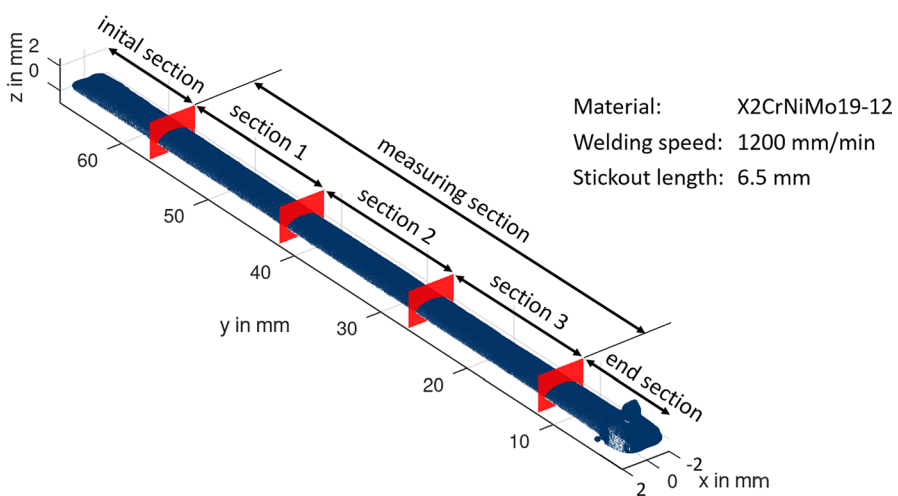
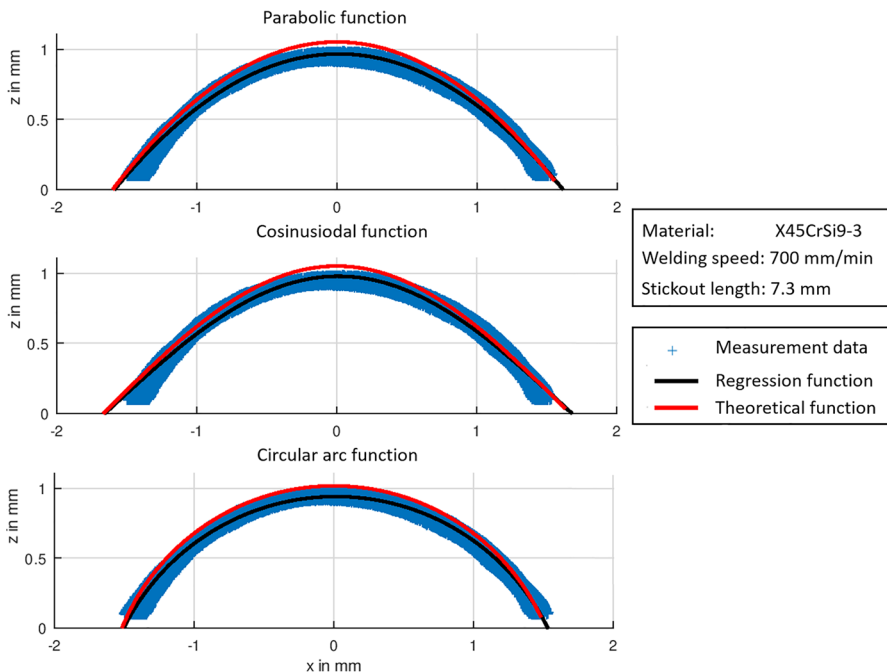**Fig. 6** Data points of the weld seam surface with different sections for the data preparation

The model functions $f_{\sigma,100}(x)$, $\sigma \in \{p, c, a\}$ for 100 % utilization were calculated and presented in addition to the fitted model functions $f_\sigma(x)$ in the analysis to allow quick visual detection of the deviation between the two functions. The parameters of the functions were determined by a system of equations based on the cross sectional area A_{100} and the zeros x_{01} and x_{02} of the fitted functions $f_\sigma(x)$:

$$f_{\sigma,100}(x_{01}) = f_{\sigma,100}(x_{02}) = 0$$

$$\int_{x_{01}}^{x_{02}} f_{\sigma,100}(x)\, dx = A_{100} \tag{7}$$

By definition the cross sectional area of the $f_{\sigma,100}$ functions equals the area as expected by the actual wire feed speed according to (6) .

Results and Discussion

The SER of the model functions was determined for all sections of all samples. Figure 7 shows the results of the analysis for one particular weld seam. The theoretical 100 % utilization model functions $f_{\sigma,100}$ are also shown to compare the cross sectional area of the regression and the cross sectional area based on the wire feed

Fig. 7 Model functions $f_{\sigma,100}$ derived for as subsection of a weld seam based on a theoretical 100 % utilization of the wire and f_σ based on a fitting to data points of a subsection of a weld seam surface

speed visually. In Fig. 7 the welding speed was 700 mm/min at a stickout length of 7.3 mm. The wire material was X45CrSi9-3.

The investigation of the suitability of the different functions for describing the weld seam geometry was carried out in different stages with different levels of detail. In this way, in addition to a general analysis on a broad data basis a detailed analysis of individual effects can be performed but with reduced sample size.

First, an analysis of variance of the SER was performed across all 162 measuring sections regardless the material and parameter combinations with a confidence level of 0.05. The results of the analysis are shown in Fig. 8. The SER ranges from 9.8 µm to 62.0 µm. With an average of 25.3 µm the circular arc function has a significantly lower SER than the cosinusiodal and parabolic functions. The cosinusiodal function has the highest SER with an average of 33.5 µm.

In order to determine whether the wire material has an influence on the weld seam geometry, the different material combinations are analyzed separately. For each wire material 54 measuring sections are available for evaluation. In all cases, the circular arc model function f_a is significantly better for describing the weld seam geometry than the cosinusiodal and the parabolic function. The cosinusiodal function always performed worst for all three materials. For X2CrNiMo19-12 wire specimen the difference in the mean SER of the weld seam model functions is particularly large (see Table 4). The circular arc function has a mean SER of 22.4 µm, while the parabolic and cosinusiodal functions have values of 27.4 µm and 32.3 µm, respectively. The SER differences of the different model functions is smallest for the X45CrSi9-3 wire material, but it is still significant. An overview of the mean SER depending on wire material and model function is given in Table 4 and Fig. 9.

In order to determine whether a process parameter has an effect on the model function shape each parameter combination of wire material, welding speed and stickout length was analyzed separately and the mean SER of the model functions
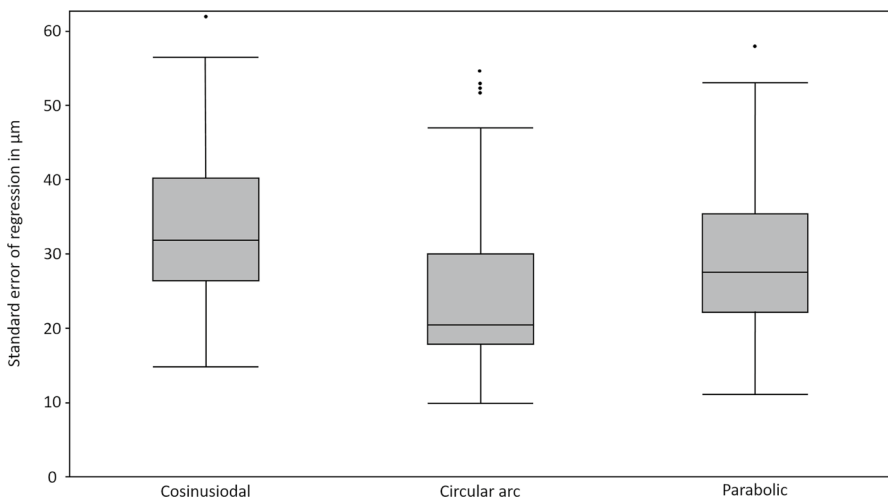
Fig. 8 Standard error of regression (SER) of the model functions
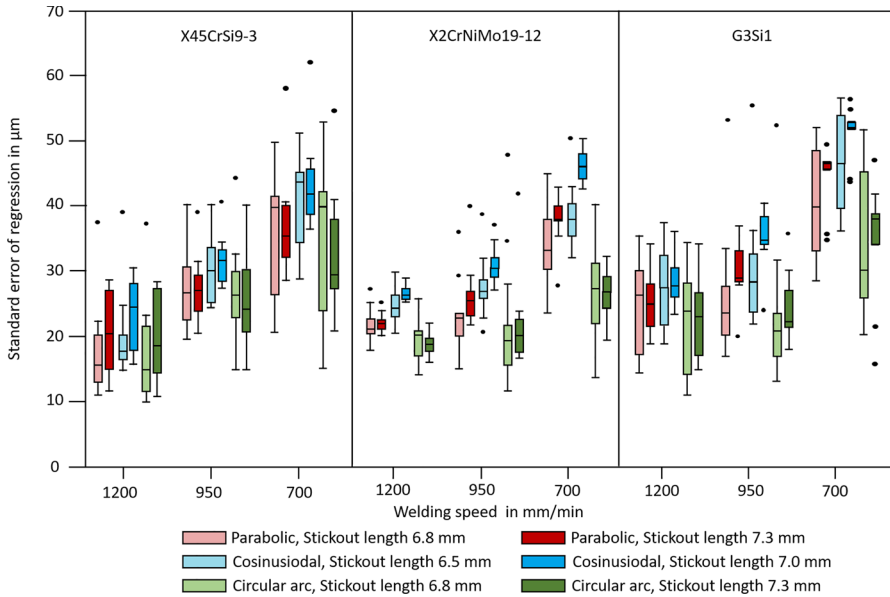
Table 4 Standard error of regression depending on wire material and model function shape

Wire material	Model function shape	Mean standard error of regression in µm
G3Si1	Parabolic	31.9
	Cosinusiodal	36.5
	Circular arc	27.2
X45CrSi9-3	Parabolic	27.8
	Cosinusiodal	31.7
	Circular arc	26.2
X2CrNiMo19-12	Parabolic	27.4
	Cosinusiodal	32.3
	Circular arc	22.4
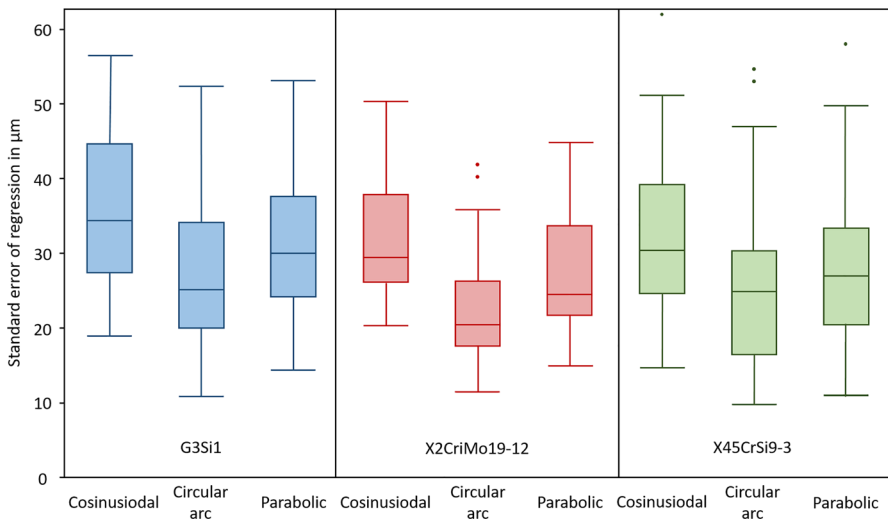
Fig. 9 Standard error of regression of the model function shape and all materials

was examined for significance. The SER is shown in Fig. 10 and the significance value p of the model functions depending on the parameter set is shown in Table 5. Nine weld seam sections were available for each parameter set for this detailed analysis.

In the case of the wire material X2CrNiMo19-12, five of six parameter combinations are below the significance level of 0.05. In one case, the value of 0.058 is only slightly above the limit. Therefore, a significantly better description of the weld seam geometry by the circular arc function can be assumed, independent of the parameter set. For the wire material G3Si1, three parameter sets are below the significance level of 0.05 and three sets are distinctly above it. Even in the parameter sets where the circular arc does not have a significantly lower SER,

Fig. 10 Standard error of regression in dependence of the parameters wire material, welding speed, stickout length and model function shape

Table 5 Significance value p of the mathematical functions in dependence of the parameters wire material, stickout length and welding speed

Wire material	Stickout length l_W in mm	Welding speed v_S in mm/min	Significance p
G3Si1	6.8	700	0.0416
	6.8	950	0.4557
	6.8	1200	0.3596
	7.3	700	0.0002
	7.3	950	0.0011
	7.3	1200	0.1869
X45CrSi9-3	6.8	700	0.4703
	6.8	950	0.5753
	6.8	1200	0.7463
	7.3	700	0.0438
	7.3	950	0.1038
	7.3	1200	0.5112
X2CrNiMo19-12	6.5	700	0.0064
	6.5	950	0.0580
	6.5	1200	0.0084
	7.0	700	0.0001
	7.0	950	0.0117
	7.0	1200	0.0001

the circular arc function still has the lowest SER. For the parameter sets with the wire material X45CrSi9-3, with one exception, the circular arc functions are not significantly better for describing the weld seam geometry but it is still the mathematical function with the lowest SER. As already shown in Table 4, where the welding parameter variation was not considered, X45CrSi9-3 is the material with the lowest significance for the circular arc function.

The reason for the occurrence of non-significances in analysis of the parameter influences on weld seam geometry might be the reduced sample size. While 162 weld seam sections are included in the analysis without taking material and welding parameters into account, only nine weld seam sections per parameter set are included in the analysis in which the influence of welding parameters and wire material is taken into account. Due to the reduced sample size, the confidence interval of the mean value increases significantly, which leads to a lower significance value. However, the trend is clearly evident for all parameter combinations at all levels of detail. Increasing the sample size probably also leads to evidence of significance for the circular arc.

Regardless of the wire material, the circular arc has the lowest SER while the parabolic function is second most suitable. A higher welding speed leads to a statistical significantly lower SER while a higher stickout length leads to a significantly higher SER. But in all cases the circular arc has the lowest standard error and therefore the circular arc is most suitable of the three model functions to describe the shape of the weld seam.

In case the wire speed remains unchanged, the weld seam height is reduced when increasing the the welding speed. Since the SER also decreases with increasing welding speed, the weld seam height is therefore related to the SER in the following, in order to check if the relative deviation is constant for all welding speeds. The weld seam heights were computed using the circular arc regression functions and the relative height error was defined by the ratio of the SER and the computed weld seam height. The relative height error ranged from 1.1 % to 6.9 %, with a mean of 3.3 %. An influence of the welding speed on the relative error could not be determined. Due to the small relative errors, it can be concluded that the circular arc function is well suited to describe the weld seam geometries studied in this paper. The model function of the weld seam surface typically used in the state of the art strongly depends on the deposition welding process, the system equipment used, and in some cases also on the welding parameters. Xiong et al. also determined a circular arc function to be the most appropriate function for high ratios of wire feed speed to welding speed when using a WAAM process [11]. Shi et al. (LMD-W), El Cheikh et al. (LMD-P) and Pinkerton and Li (LMD-P) used the circular arc as the mathematical function to describe the weld seam geometry and achieved good agreement [8, 9, 17]. Based on the data from the wire feed unit the actual wire feed speed of each weld seam can be determined. A wire feed speed of 2.0 m/min was set for all weld seams. The recorded data showed that an average actual speed of 1.973 m/min was reached. The theoretical 100 % utilization cross section A_{100} was calculated according to Eq. 6 and compared to the experimental cross section A_M which was determined by integration of the circular arc fit function. The deviation α between

experimental and theoretical 100 % utilization cross sectional area was calculated by the following equation:

$$\alpha = \frac{A_{100} - A_{\mathrm{M}}}{A_{100}} \tag{8}$$

A mean deviation of $\overline{\alpha} = 10.62$ % was determined. A statistical analysis showed that the wire material has no significant influence on α while significant influences of the welding speed and the stickout length were found. Typically, a higher welding speed leads to a reduction of the cross sectional area but also to an increase in α (see Fig. 11). At the same time α reduces if the wire stickout length is increased. These observations were independent on the position along the weld seam as the result for different sections indicate.

The reason for the dependency of α on the wire feed speed is not clear at the moment and requires further investigation. A possible reason could be the separation of substrate points and weld seam surface points in the preparation of the point clouds. The Δ tolerance based criterion is an approximation that can lead to deviations in the determination of the cross sectional area. Another factor that should be examined more closely is the actual wire feed speed. It is measured in the drive unit of the wire feed unit, which is located several hundred millimeters away from the welding spot. Due to the long feeding distance, a slight wire jam could possibly go unnoticed by the wire feed speed sensor system.
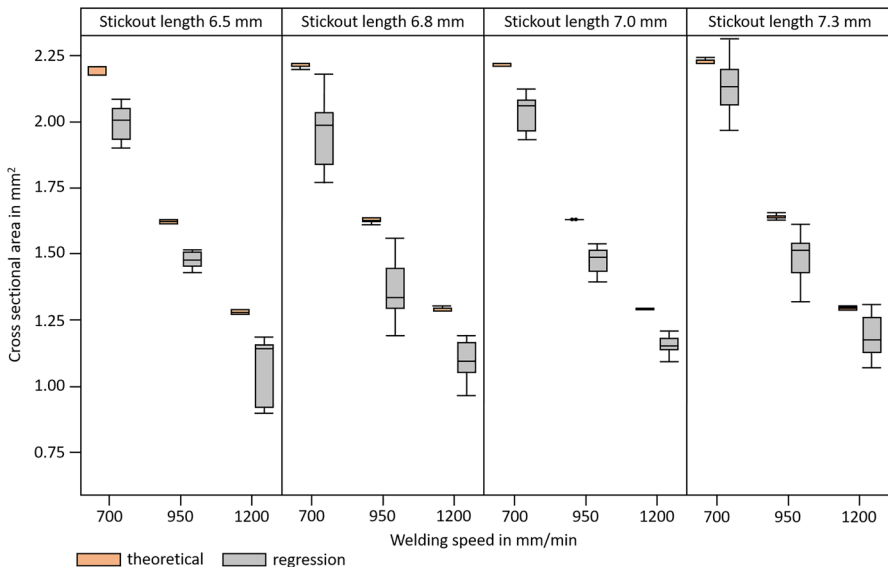
Fig. 11 Theoretical 100 % utilization cross sectional area and regression based cross sectional area of an integrated fit function in dependence of the welding speed and the stickout length

Conclusion

The investigation of weld seams made of three different materials and with different process parameters has shown that the circular arc function is in all cases best suited to describe the shape of the weld seam manufactured by coaxial laser hotwire deposition welding with the welding head MK-II, manufactured by Laser Zentrum Hannover e.V.. For the three examined wire materials and the three model functions used, the circular arc function was the most appropriate function to describe the geometry of the weld seam surface. When the welded specimen are categorized into single factors based on their welding parameters and the wire material, differences become visible. A different degree of significance for the standard error of regression (SER) of the circular arc function was found depending on the material. The lowest values of significance p in the range of 0.0001 to 0.0580 were obtained for the wire material X2CrNiMo19-12. The shape of the model function describing the weld seam geometry best is not influenced by welding speed or stickout length but these welding parameters influence the SER, which is used to describe how well the regression function fits. When increasing welding speed the SER reduces while increasing stickout length increases the SER. The relative error of regression is independent of the welding parameters at an average value of 3.3 %. The cross sectional area of the regression fit function and the area function assuming a 100 % utilization of the wire material differ depending on the wire feed speed and the wires stickout length, but it does not dependent on the wire material or the weld seam position. The relative deviation of both is reduced when increasing the wire stickout length or reducing the welding speed.

As an overall result the investigation suggests further research concerning the influences on the cross sectional area. The investigations also lay the foundation for developing models describing the shape of adjacent weld seams. Here it is important to check whether the circular arc function also describes the weld seam geometry well for overlapping weld seams. Such a model can then be used to predict the waviness of a cladding, which is important for subsequent machining processes.

Author Contributions Laura Budde, Kai Biester and Michael Huse contributed to the study conception and design. Material preparation, data collection and analysis were performed by Laura Budde and Kai Biester. The first draft of the manuscript was written by Laura Budde and Kai Biester and all authors commented on previous versions of the manuscript. All authors read and approved the final manuscript.

Data Availability The datasets generated during and/or analysed during the current study are not publicly available but are available from the corresponding author on reasonable request.

Declarations

References

1. Saha, M.K., Das, S.: A review on different cladding techniques employed to resist corrosion. Journal of the Association of Engineers, India **86**(1–2), 51 (2016)
2. Kaierle, S., Barroi, B., Noelke, C., Hermsdorf, J., Overmeyer, L., Haferkamp, H.: Review on laser deposition welding: From Micro to Macro. Physics Procedia **39**, 336–345 (2012)
3. Dutta, B., Babu, S., Jared, B.: Additive manufacturing technology. In: Science, Technology and Applications of Metals in Additive Manufacturing, pp. 11–53. Elsevier (2019)
4. Ocelík, V., Nenadl, O., Palavra, A., De Hosson, J.T.M.: On the geometry of coating layers formed by overlap. Surface and Coatings Technology **242**, 54–61 (2014)
5. Nenadl, O., Ocelík, V., Palavra, A., De Hosson, J.T.M.: The prediction of coating geometry from main processing parameters in laser cladding. Physics Procedia **56**(C), 220–227 (2014)
6. Nenadl, O., Kuipers, W., Koelewijn, N., Ocelík, V., Th, J., De Hosson, M.: A versatile model for the prediction of complex geometry in 3D direct laser deposition. Surface and Coatings Technology **307**, 292–300 (2016)
7. Gonçalves, D.A., Stemmer, M.R., Pereira, M.: A convolutional neural network approach on bead geometry estimation for a laser cladding system. The International Journal of Advanced Manufacturing Technology **106**(5–6), 1811–1821 (2020)
8. El Cheikh, H., Courant, B., Branchu, S., Hascoët, J.Y., Guillén, R.: Analysis and prediction of single laser tracks geometrical characteristics in coaxial laser cladding process. Optics and Lasers in Engineering **50**(3), 413–422 (2012)
9. Shi, J., Zhu, P., Fu, G., Shi, S.: Geometry characteristics modeling and process optimization in coaxial laser inside wire cladding. Optics & Laser Technology **101**, 341–348 (2018)
10. Ding, D., Pan, Z., Cuiuri, D., Li, H.: A multi-bead overlapping model for robotic wire and arc additive manufacturing (WAAM). Robotics and Computer-Integrated Manufacturing **31**, 101–110 (2015)
11. Xiong, J., Zhang, G., Gao, H., Wu, L.: Modeling of bead section profile and overlapping beads with experimental validation for robotic GMAW-based rapid manufacturing. Robotics and Computer-Integrated Manufacturing **29**(2), 417–423 (2013)
12. Cao, Y., Zhu, S., Liang, X., Wang, W.: Overlapping model of beads and curve fitting of bead section for rapid manufacturing by robotic MAG welding process. Robotics and Computer-Integrated Manufacturing **27**(3), 641–645 (2011)
13. Deng, J., Xu, Y., Zuo, Z., Hou, Z., Chen, S.: bead geometry prediction for multi-layer and multi-bead wire and Arc additive manufacturing based on XGBoost. In: Transactions on Intelligent Welding Manufacturing, pp. 125–135. Springer, Singapore (2019)
14. Karmuhilan, M., Sood, A.K.: Intelligent process model for bead geometry prediction in WAAM. Materials Today: Proceedings **5**(11), 24005–24013 (2018)

15. Xue, Q., Ma, S., Liang, Y., Wang, J., Wang, Y., He, F., Liu, M.: Weld bead geometry prediction of additive manufacturing based on neural network. Proceedings - 2018 11th International Symposium on Computational Intelligence and Design, ISCID 2018, 2:47–51 (2018)

16. Wei, S., Wang, G., Shin, Y.C., Rong, Y.: Comprehensive modeling of transport phenomena in laser hot-wire deposition process. International Journal of Heat and Mass Transfer **125**, 1356–1368 (2018)

17. Pinkerton, A.J., Li, L.: Modelling the geometry of a moving laser melt pool and deposition track via energy and mass balances. Journal of Physics D: Applied Physics **37**(14), 1885–1895 (2004)

18. Ríos, S, Colegrove, PA., Martina, F, Williams, SW.: Analytical process model for wire + arc additive manufacturing. Additive Manuf, 21 (2018)

19. Thyssenkrupp. precidur® S235JR/J0/J2

20. Linde Welding GmbH. Sicherheitsdatenblatt

21. Deutsche Edelstahlwerke. Werkstoffdatenblatt X45CrSi9-3 - 1.4718 (2016)

22. Rotek Handels GmbH. Draht-/Stabelektrode - E316L/1.4430 zum Schweißen nichtrostender und kaltzäher austenitischer Stähle (2008)

23. Steel Grades. ER 70 S-6

24. Deutsche Edelstahlwerke. Werkstoffdatenblatt X2CrNiMo18-14-3 - 1.4435 (2015)

25. Lammers, M., Hermsdorf, J., Kaierle, S., Ahlers, H.: Entwicklung von Laser-Systemkomponenten für das koaxiale Laser-Draht-Auftragschweißen von Metall- und Glaswerkstoffen. In: Lachmayer, R., Rettschlag, K., Kaierle, S. (eds.) Konstruktion für die Additive Fertigung 2019, pp 245–260. Springer, Berlin Heidelberg, Berlin, Heidelberg (2020)

26. Pajukoski, H., Näkki, J., Thieme, S., Tuominen, J., Nowotny, S., Vuoristo, P.: High performance corrosion resistant coatings by novel coaxial cold- and hot-wire laser cladding methods. Journal of Laser Applications **28**(1), 012011 (2016)

27. Gavin, H.P.: The levenberg-marquardt algorithm for nonlinear least squares curve-fitting problems. Duke University, pp. 1–19 (2019)